JOURNAL OF SOLID STATE CHEMISTRY **140,** 116–127 (1998)
ARTICLE NO. SC987873

Structural Features of Low-Temperature $LiCoO_2$ and Acid-Delithiated Products

Y. Shao-Horn[1] and S. A. Hackney[2]

Department of Metallurgical & Materials Engineering, Michigan Technological University, Houghton, Michigan 49931

and

C. S. Johnson, A. J. Kahaian, and M. M. Thackeray

Electrochemical Technology Program, Chemical Technology Division, Argonne National Laboratory, Argonne, Illinois 60439

Received December 24, 1997; in revised form April 21, 1998; accepted April 28, 1998

X-ray diffraction and transmission electron microscopy were used to study the structural features of low-temperature $LiCoO_2$ (LT-$LiCoO_2$) samples prepared at 400°C either by a simple solid-state reaction or via a sol–gel process. Single-crystal electron diffraction analysis showed that both a lithiated-spinel $Li_2[Co_2]O_4$ (*Fd3m*) and a layered-type structure ($R\bar{3}m$) were present in LT-$LiCoO_2$ samples but that the lithiated-spinel structure was the major phase. Electron diffraction analysis also indicated that some crystallites in the LT-$LiCoO_2$ samples had a cation distribution in the spinel notation, $\{(Li_{16-4x})_{16c}[Li_{4x}]_{16d}\}_{layer1}\{(Co_{16-4x})_{16d}[Co_{4x}]_{16c}\}_{layer2}O_{32}$ ($0<x<1$) that was intermediate between the ideal layered ($x=1$) and ideal lithiated-spinel ($x=0$) structures. Electron diffraction confirmed that acid-delithiation of LT-$LiCoO_2$ resulted in a lithium-deficient spinel, $Li_{0.8}[Co_2]O_4$, with lithium ions on the tetrahedral sites of the spinel structure. The structural features of LT-$LiCoO_2$ and the acid-delithiated $Li_{0.4}CoO_2$ products provide reasons for the poor electrochemical properties of Li/LT-$LiCoO_2$ cells and are consistent with earlier studies. © 1998 Academic Press

Key Words: **low-temperature lithium cobalt oxide; crystal structure; transmission electron microscopy, electron diffraction.**

INTRODUCTION

Considerable efforts have been made previously to evaluate a "low-temperature" form of $LiCoO_2$ (LT-$LiCoO_2$) synthesized at 400°C as a positive electrode material for lithium batteries (1–9). LT-$LiCoO_2$ has been reported to have very poor electrochemical properties, in contrast to the superior electrochemical performance of "high-temperature" $LiCoO_2$ (HT-$LiCoO_2$) synthesized typically at 800°C (1, 10). Attempts have been made to correlate the electrochemical properties with the crystal structure of LT-$LiCoO_2$. Analysis of neutron diffraction data has provided evidence that the averaged structure of LT-$LiCoO_2$ can be regarded as one that is intermediate between a layered $LiCoO_2$ structure ($R\bar{3}m$) and a lithiated-spinel $Li_2[Co_2]O_4$ structure (*Fd3m*) (1, 3, 4). By contrast, the delithiated product obtained by the acid digestion of LT-$LiCoO_2$ at room temperature has been reported to be a single-phase defect spinel, $Li_{0.8}[Co_2]O_4$ [Li_yCoO_2 ($y=0.4$)] (1, 4). Other research groups have concluded from electrochemical studies (6, 7) and vibrational spectroscopy (8) that LT-$LiCoO_2$ has only the lithiated-spinel $Li_2[Co_2]O_4$ structure (*Fd3m*). The difficulty in the interpretation of the diffraction data arises from he strong similarity between the X-ray and neutron powder diffraction patterns of layered $LiMO_2$ and lithiated-spinel $Li_2[M_2]O_4$ structures (M = transition metal cation). If the oxygen arrays are ideally cubic-close packed ($c/a=4.899$), the X-ray and neutron diffraction patterns are indistinguishable (6, 7). This ambiguity does not exist for perfectly layered structures such as HT-$LiCoO_2$ because, in general, the oxygen arrays are not quite ideally cubic-close-packed. For example, HT-$LiCoO_2$ has a c/a of 4.99 (10, 11); in this case, it is reasonably easy to identify the layered structure. However, it is more difficult to distinguish structures with cation distributions between those of the ideal layered and ideal spinel configurations, particularly when the c/a ratio approaches 4.899.

One approach to resolve the problems associated with the structure interpretation of X-ray and neutron powder diffraction analyses is to use single-crystal diffraction techniques. For example, in structures with ideal cubic-close packed arrays, the symmetry of the (110) reciprocal lattice plane in a lithiated-spinel structure (*Fd3m*) is different from

[1] Present address: Energizer/c.q, 25225 Detroit Road, P.O. Box 450777, Westlake, OH 44145. E-mail: Yang.ShaoHorn@Energizer.com.

[2] To whom correspondence should be addressed. E-mail: Hackney@mtu.edu.

0022-4596/98 $25.00

that of the corresponding (010) reciprocal lattice plane in a layered structure ($R\bar{3}m$) (6, 7). It should be possible, therefore, for single-crystal electron diffraction analysis to distinguish a lithiated-spinel from a layered structure. Furthermore, it should be possible to determine whether LT-$LiCoO_2$ is a single-phase, lithiated-spinel product or whether it has a structure with an intermediate cation distribution between layered $LiCoO_2$ and lithiated-spinel $Li_2[Co_2]O_4$. Because the crystallite sizes of LT-$LiCoO_2$ are too small for selected area electron diffraction to obtain single-crystal electron diffraction patterns, convergent beam electron diffraction (spatial resolution down to 5 nm) in a transmission electron microscope is used in this study.

In addition to the ambiguity in the interpretation of the X-ray and neutron diffraction data, a further source of confusion in the literature is the sensitivity of the structure LT-$LiCoO_2$ to the processing technique. This sensitivity necessitates an examination of the structural features of LT-$LiCoO_2$ products prepared by different processing routes. In this paper, we report on the analyses of LT-$LiCoO_2$ samples, prepared at 400°C either by a solid-state reaction or via a sol–gel process using convergent beam electron diffraction and high-resolution lattice imaging in combination with X-ray diffraction analysis. An acid-delithiated product from LT-$LiCoO_2$ prepared by the solid-state reaction is also studied similarly to determine the effects of acid-delithiation on the structure. This approach attempts to resolve the conflicting debate in the literature about the structural properties of LT-$LiCoO_2$ products.

EXPERIMENTAL

HT-$LiCoO_2$ and LT-$LiCoO_2$ samples were prepared as described in the literature (1, 9, 12). The HT-$LiCoO_2$ sample was prepared by heating Li_2CO_3 and $CoCO_3$ at 850°C in air for 1 day (12). LT-$LiCoO_2$ materials were prepared by two different synthesis methods. The first method involves a solid-state reaction of Li_2CO_3 and $CoCO_3$ at 400°C in air for 10 days (1); the final product is denoted as LT-$LiCoO_2$ (SS). The second method is a sol–gel process (9) followed by heat treatments at 400°C in air for up to 4 days with intermediate grinding; the final product is denoted LT-$LiCoO_2$ (SG).

LT-$LiCoO_2$ (SS) was digested in 2.5 M sulfuric acid for 8 h at room temperature. In the acid digestion reaction, the gram weight to milliliter volume ratio of oxide powder to acid was 1 : 10; the powder was continuously stirred throughout the entire reaction period. After it was washed to a neutral pH with purified water (Milli-Q, Millipore Corp.), the acid-delithiated product was dried at 100°C for 24 h. Cobalt and lithium contents in the delithiated sample were determined by inductively coupled plasma atomic emission spectroscopy (ICP-AES) on an Instruments SA JY86 spectrometer system. The delithiated product was found to have a Li/Co ratio of 0.38.

X-ray powder diffraction data on HT-$LiCoO_2$, LT-$LiCoO_2$ materials, and the acid-delithiated product were obtained on an automated Siemens D5000 powder diffractometer with CuK_α radiation. These materials were also examined by high-resolution lattice imaging and convergent beam electron diffraction on a transmission electron microscope (JEOL-JEM 4000FX-1) under an accelerating voltage of 200 keV. All samples studied in this study were stable under the electron beam during analysis.

RESULTS AND DISCUSSION

X-Ray Diffraction Analysis

X-ray diffraction patterns of HT-$LiCoO_2$, LT-$LiCoO_2$ (SS), LT-$LiCoO_2$ (SG), and LT-$Li_{0.38}CoO_2$ (SS) are shown in Fig. 1a–d, respectively. The pattern (Fig 1a) of HT-$LiCoO_2$ is indexed according to the trigonal symmetry ($R\bar{3}m$) while that (Fig. 1b) of LT-$LiCoO_2$ (SS) is indexed to the lithiated-spinel $Li_2[Co_2]O_4$ structure with space group $Fd3m$. The X-ray diffraction peaks of LT-$LiCoO_2$ (SS) and LT-$Li_{0.38}CoO_2$ (SS) are broader than those of HT-$LiCoO_2$, indicative of smaller crystallites and perhaps greater strain in the LT-$LiCoO_2$ materials. Lattice parameters, as determined from the least-squares refinement of peak positions in the X-ray diffraction patterns in Fig. 1, and c/a ratios for the four $LiCoO_2$ materials, are listed in Table 1; these data are in good agreement with those reported in the literature (1–4, 10, 11). The c/a ratios of LT-$LiCoO_2$ (SS) and LT-$LiCoO_2$ (SG) are significantly smaller than that of HT-$LiCoO_2$ but are close to the ideal c/a ratio of 4.899 for cubic-close-packed structures. It is significant to note that of

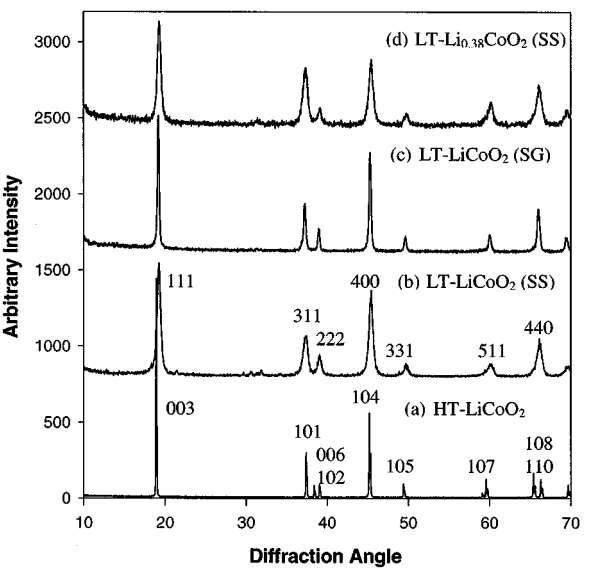

FIG. 1. X-ray diffraction patterns of (a) HT-$LiCoO_2$, (b) LT-$LiCoO_2$ (SS) with some unreacted Li_2CO_3, (c) LT-$LiCoO_2$ (SG), and (d) LT-$Li_{0.38}CoO_2$ (SS) using Cu$K\alpha$ radiation.

TABLE 1
Lattice Parameters of HT-$LiCoO_2$, LT-$LiCoO_2$ and an Acid-Delithiated Product of LT-$LiCoO_2$

Sample	a (Å)	c (Å)	c/a
HT-$LiCoO_2$	2.813(8)	14.040(0)	4.989(9)
LT-$LiCoO_2$ (SS)	2.823(3)	13.853(4)	4.906(8)
LT-$LiCoO_2$ (SG)	2.828(3)	13.870(6)	4.904(2)
LT-$Li_{0.38}CoO_2$ (SS)	2.826(3)	13.846(3)	4.899(0)

all the four samples, the c/a ratio of the acid-treated sample, LT-$Li_{0.38}CoO_2$, was the only one that corresponded exactly with the ideal cubic-close-packed value.

Transmission Electron Microscope Imaging

Transmission electron microscope images of HT-$LiCoO_2$, LT-$LiCoO_2$ (SS), LT-$LiCoO_2$ (SG), and the acid-delithiated product, LT-$Li_{0.38}CoO_2$ (SS) are shown in Fig. 2a–d, respectively. It should be noted that only crystallite agglomerates could be resolved for LT-$LiCoO_2$ and LT-$Li_{0.38}CoO_2$ products in Fig. 2. The individual crystallites of LT-$LiCoO_2$ (SS), LT-$LiCoO_2$ (SG), and LT-$Li_{0.38}CoO_2$ (SS) are shown in the high-resolution lattice images (Fig. 3a–c). These images of individual crystallites allow the direct measurement of the projected crystallite area. Frequency distributions of the projected crystallite area obtained from transmission electron microscope images of these four

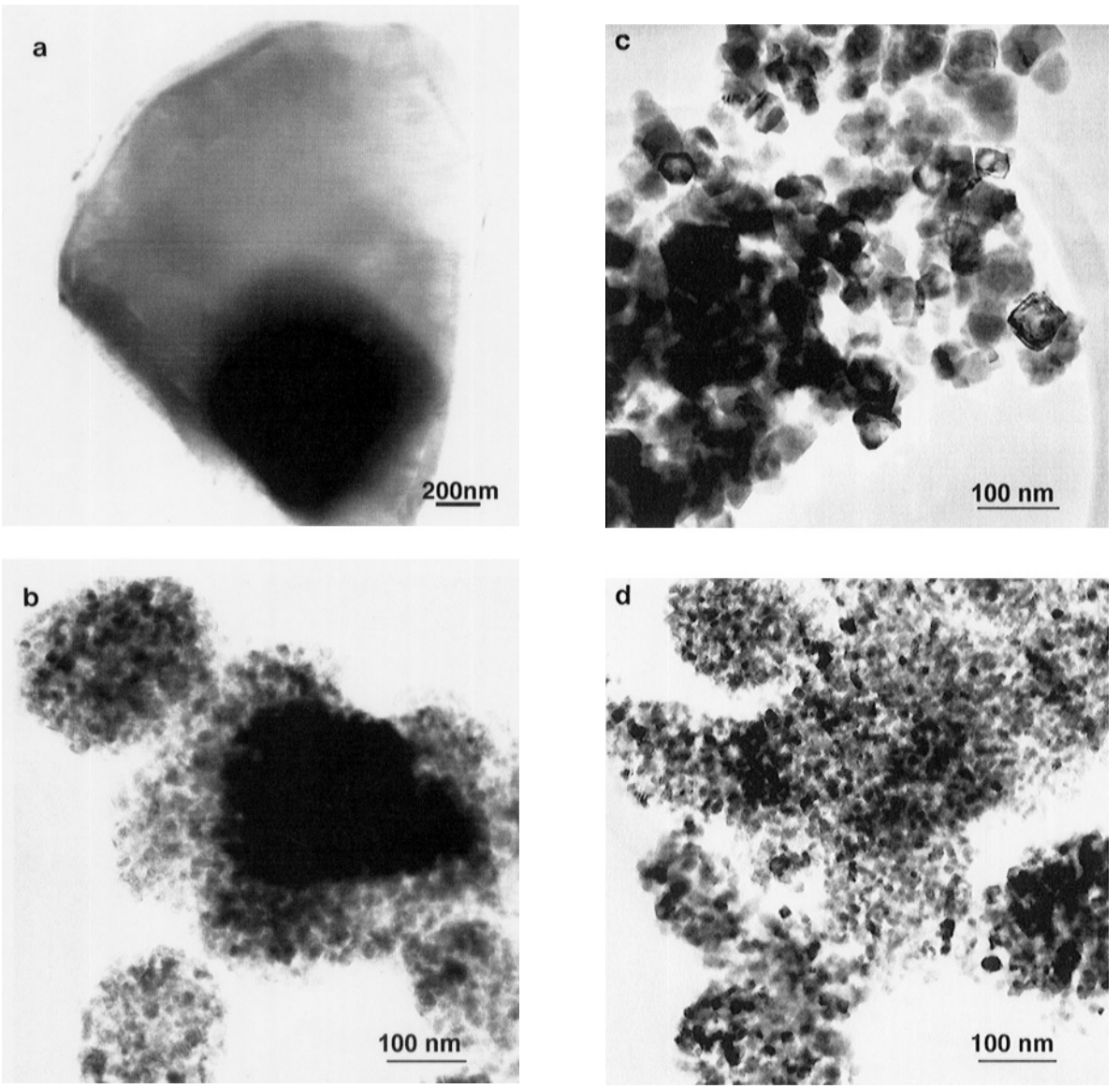

FIG. 2. Transmission electron microscope images of (a) HT-$LiCoO_2$, (b) LT-$LiCoO_2$ (SS), (c) LT-$LiCoO_2$ (SG), and (d) LT-$Li_{0.38}CoO_2$ (SS).

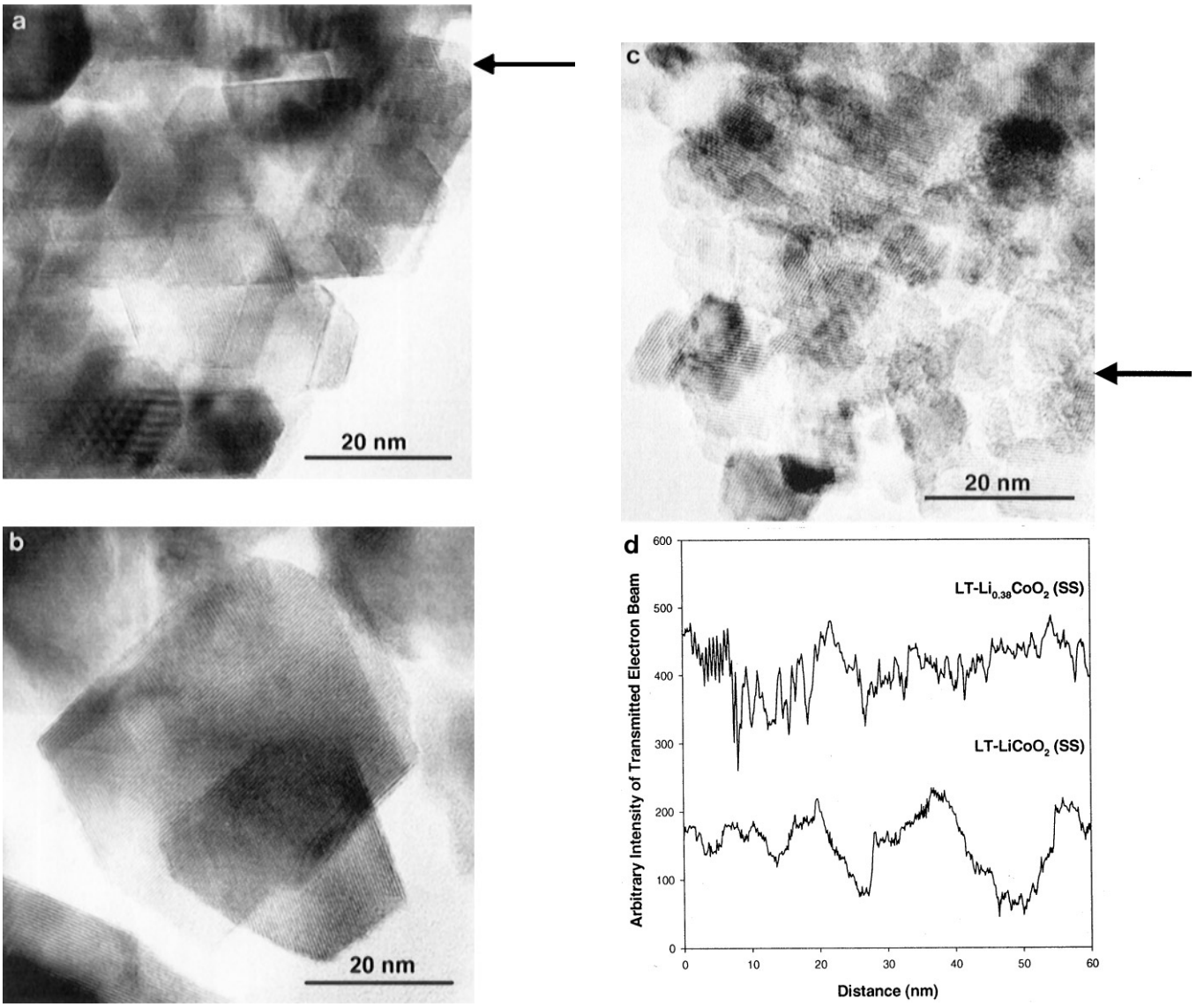

FIG. 3. High-resolution transmission electron microscope images of (a) LT-$LiCoO_2$ (SS), (b) LT-$LiCoO_2$ (SG), and (c) LT-$Li_{0.38}CoO_2$ (SS); (d) the variations in the transmitted electron beam intensity corresponding to (a) and (c), which was digitized horizontally from the points marked by arrows in (a) and (c), respectively.

materials are plotted in Fig. 4a–d. The projected crystallite area of a HT-$LiCoO_2$ crystallite was calculated from the product of the longest dimension and the shortest dimension of the crystallite because the shapes of HT-$LiCoO_2$ crystallites appeared to be uniform. The transmission electron microscope images of LT-$LiCoO_2$ crystallites demonstrate a variety of faceted geometrical shapes, including rods, plates, etc. In order to provide a consistent measurement of the projected crystallite area, only rod-shaped crystallites of LT-$LiCoO_2$ products were considered in the measurements and the projected crystallite area was calculated from the product of the rod length and rod width. As expected from the processing temperature, HT-$LiCoO_2$ has a significantly larger average crystallite area (approximately 10^7 nm^2) relative to LT-$LiCoO_2$ (SS), LT-$LiCoO_2$ (SG), and LT-$Li_{0.38}CoO_2$ (SS) samples (10^2–10^4 nm^2). Although the crystallite morphology of LT-$LiCoO_2$ (SS) (Fig. 3a,b) is similar to that of the LT-$LiCoO_2$ (SG), the average crystallite area of LT-$LiCoO_2$ (SS) is smaller than that for LT-$LiCoO_2$ (SG). These data, therefore, highlight the difference in morphological features of $LiCoO_2$ products that are obtained when different synthesis techniques are employed.

Provided that LT-$LiCoO_2$ (SS) has an average crystallite size of 20 nm (as determined from transmission electron

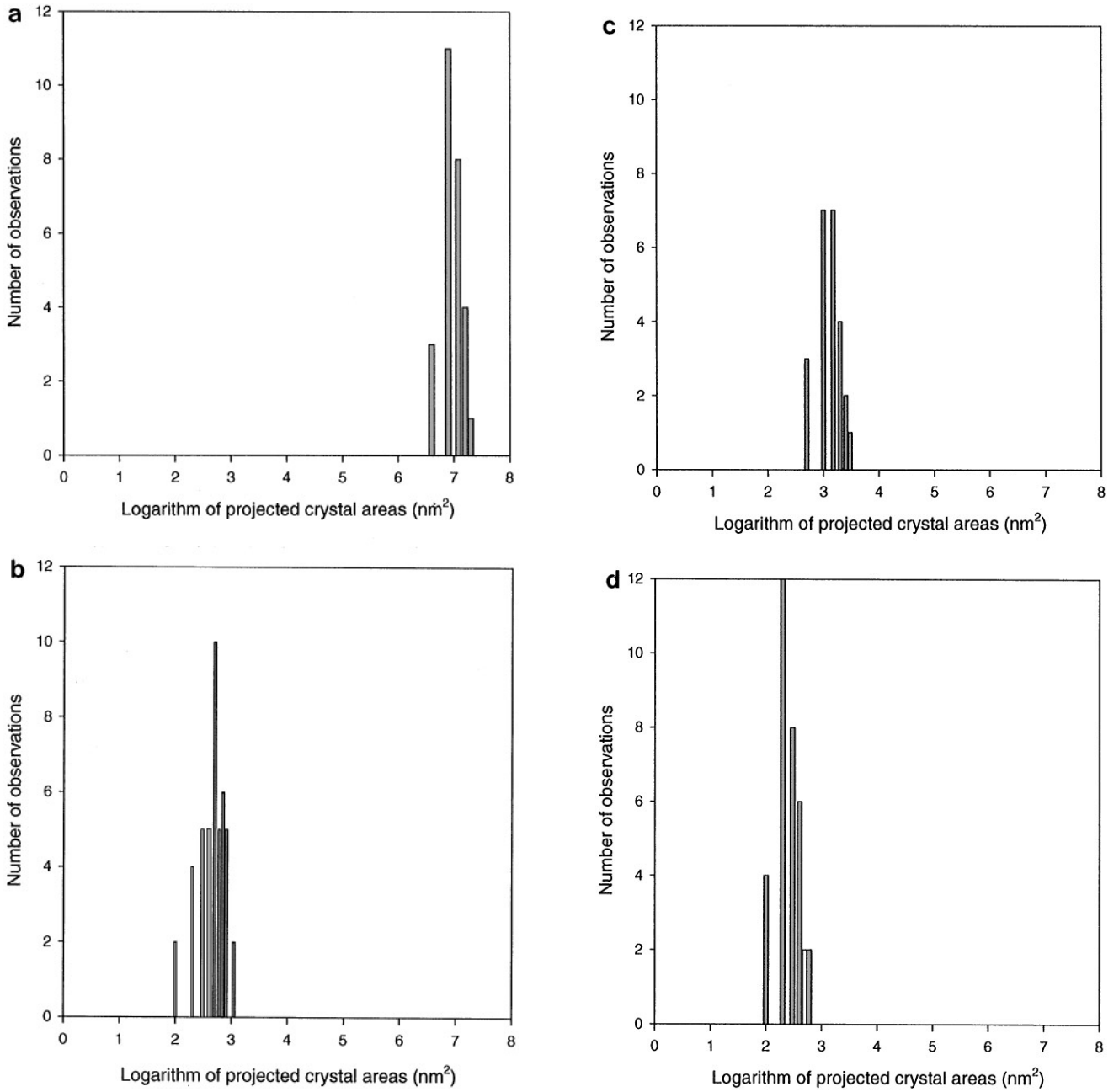

FIG. 4. Histograms of projected crystallite areas of (a) HT-$LiCoO_2$, (b) LT-$LiCoO_2$ (SS), (c) LT-$LiCoO_2$ (SG), and (d) LT-$Li_{0.38}CoO_2$ (SS).

microscope images), the Scherrer equation (13) predicts that the width of the first X-ray diffraction peak at 19.2° (2θ) should be 0.4° (2θ) at half-maximum intensity. This value is consistent with the observed peak width of 0.45° (2θ) in the X-ray diffraction pattern of LT-$LiCoO_2$ (SS) (Fig. 1b), and the difference between observed and calculated 2θ values is attributed to instrumental broadening. Therefore, the peak broadening of LT-$LiCoO_2$ (SS) is attributed primarily to crystallite size effects. It should be noted that the crystallite sizes of LT-$LiCoO_2$ (SS) (Fig. 4d) were reduced during the acid treatment. The reduction in the crystallite size of the LT-$Li_{0.38}CoO_2$ sample during acid digestion resulted in further peak broadening in the X-ray diffraction pattern, as shown in Fig. 1d.

Spatial variations in the transmitted electron beam intensity of LT-$LiCoO_2$ (SS) and LT-$Li_{0.38}CoO_2$ (SS) in Fig. 3a and c are plotted in Fig. 3d. It should be noted that the noise in the intensity plot of individual LT-$Li_{0.38}CoO_2$ (SS)

crystallites is much greater than the noise in individual LT-$LiCoO_2$ (SS) crystals. This high-frequency oscillation of transmitted electron intensity and the circular defects evident in the transmission electron micrograph in Fig. 3c indicate surface roughness or porosity on the surfaces of crystallites. Transmission electron microscope observations of an acid-delithiated spinel $Li_{0.1}Mn_2O_4$ have indicated a similar development of surface roughness or porosity (14). The formation of surface roughness or porosity within a crystallite has been attributed to nonuniform dissolution in acidic media of divalent transition metal ions associated with the disproportionation reaction (14):

$$2LiMn_2O_4\ (\text{solid}) \rightarrow 3MnO_2\ (\text{solid}) + MnO\ (\text{solution}) + Li_2O\ (\text{solution}). \quad [1]$$

For the acid treatment of LT-$LiCoO_2$, the analogous, ideal reaction (15) for the formation of a spinel product would be:

$$3LiCoO_2\ (\text{solid}) \rightarrow LiCo_2O_4\ (\text{solid}) + CoO\ (\text{solution}) + Li_2O\ (\text{solution}). \quad [2]$$

Convergent Beam Electron Diffraction Analysis of LT-$LiCoO_2$

Convergent beam electron diffraction was performed on HT-$LiCoO_2$, LT-$LiCoO_2$ (SS), LT-$LiCoO_2$ (SG), and the acid-delithiated LT-$Li_{0.38}CoO_2$ (SS) samples. Over 30 single-crystal electron diffraction patterns were obtained from the two LT-$LiCoO_2$ products, and 15 electron diffraction patterns were collected from the acid-delithiated sample.

The layered and the spinel structures have been studied extensively in the past; schematic illustrations of the $[Co_2]O_4$ spinel framework and $LiCoO_2$ layered structure are shown in Fig. 5a, b. In the layered $(Li)_{3a}[Co]_{3b}O_2$ structure (space group $R\bar{3}m$), lithium and cobalt cations reside in alternate layers of octahedral sites between the cubic-close-packed oxygen arrays. The crystallographic sites for lithium and cobalt cations in the layered structure are 3*a* at (0,0,0) and 3*b* at $(0, 0, \frac{1}{2})$, respectively. In the lithiated-spinel $(Li_2)_{16c}[Co_2]_{16d}O_4$ structure (space group $Fd3m$), lithium and cobalt ions are arranged in alternating layers with a Co/Li ratio of 3 : 1 between the cubic-close-packed oxygen arrays. The crystallographic sites for lithium and cobalt cations in the lithiated-spinel structure are 16*c* at (0, 0, 0) and 16*d* at $(\frac{1}{2}, \frac{1}{2}, \frac{1}{2})$, respectively. The lithiated-spinel structure has four sets of symmetrically equivalent close-packed cobalt planes, (1 1 1), $(\bar{1}\ 1\ 1)$, $(1\ \bar{1}\ 1)$, and $(\bar{1}\ \bar{1}\ 1)$, whereas the layered structure has only one set of equivalent close-packed cobalt planes, (003).

A single-crystal electron diffraction pattern collected from HT-$LiCoO_2$ is shown in Fig. 6. This pattern is indexed along the [010] zone axis according to trigonal symmetry ($R\bar{3}m$). Figure 6 demonstrates only the characteristic symmetry of the layered structure ($R\bar{3}m$); the pattern cannot be indexed according to the cubic symmetry of the lithiated-

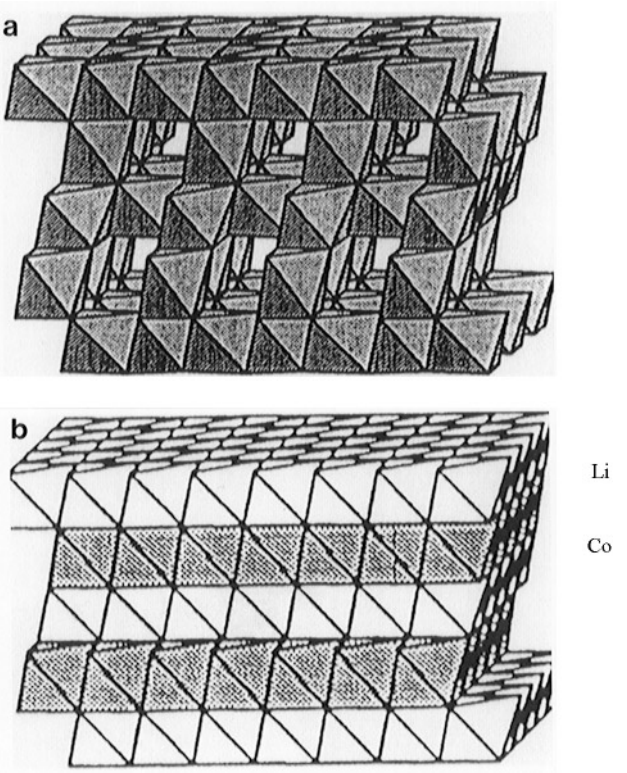

FIG. 5. Schematics of (a) the $[Co_2]O_4$ spinel framework and (b) the $LiCoO_2$ layered structure, showing different lithium and cobalt arrangements. Shaded octahedra are occupied by cobalt ions and unshaded octahedra by lithium ions.

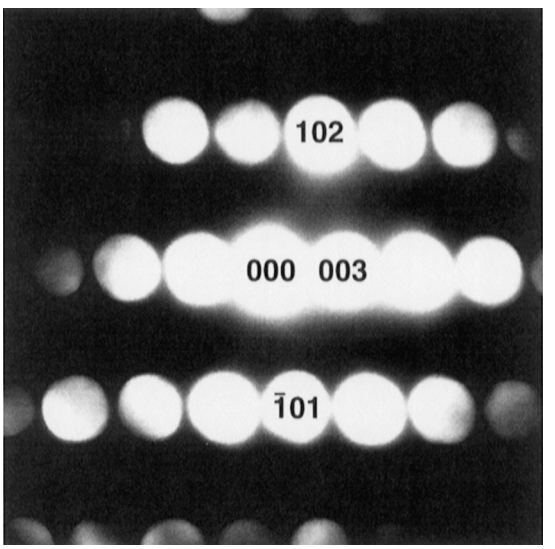

FIG. 6. A single-crystal electron diffraction pattern of HT-$LiCoO_2$, indexed according to the trigonal symmetry ($R\bar{3}m$).

spinel structure ($Fd3m$). Therefore, the layered structure can be distinguished easily from the lithiated-spinel structure using single-crystal electron diffraction.

Single-crystal electron diffraction patterns collected from two LT-$LiCoO_2$ (SS) crystallites and one LT-$LiCoO_2$(SG) crystallite are shown in Fig. 7a–c. It should be pointed out that it is very difficult to collect well-aligned, single-crystal, zone-axis patterns from LT-$LiCoCO_2$ products, especially LT-$LiCoO_2$ (SS), because the size of LT-$LiCoO_2$ crystallites is equivalent to the electron beam size used in the study. Nevertheless, useful information can still be extracted from the electron diffraction patterns of LT-$LiCoO_2$. In Fig. 7a, the diffraction pattern is indexed according to the lithiated-spinel structure with cubic symmetry ($Fd3m$) along the $[10\bar{1}]$ direction; it cannot be indexed consistently with trigonal symmetry ($R\bar{3}m$). The (111) and $(1\bar{1}1)$ reciprocal points (shown in Fig. 7a) have similar scattering intensities, as expected for an ideal lithiated-spinel structure. By contrast, although the single-crystal diffraction patterns in Fig. 7b,c show reflections at reciprocal lattice positions coincident with the pattern in Fig. 7a, the (111) and $(1\bar{1}1)$ reflections have significantly different scattering intensities. It should be noted, however, that both the (222) and $(2\bar{2}2)$ reflections in Fig. 7b,c have similar scattering intensities to those in Fig. 7a. This result indicates that the variation in the scattering intensity of the $\{111\}$ planes in Fig. 7b,c is not a result of pure misalignment of the $[10\bar{1}]$ zone axis relative to the electron beam. The scattering intensity variation observed in the $\{111\}$ planes may be explained by the following ways: (i) overlapping of a layered and lithiated-spinel crystallite with the $(111)_{\text{lithiated-spinel}}$ parallel to the $(003)_{\text{layered}}$; (ii) overlapping of two layered crystallites orientated with a $\sim 70^\circ$ angle for the (003) planes; and (iii) nonideal cation distribution intermediate between the layered and lithiated-spinel structures. However, the first two explanations are not consistent with the previous neutron diffraction and electrochemical data of LT-$LiCoO_2$ electrodes, which revealed that LT-$LiCoO_2$ had neither a single-phase layered structure nor a physical mixture of layered and lithiated-spinel crystallites (1–8). Therefore, we propose that the interpretation of the electron diffraction data most consistent with the previous work is a nonideal cation distribution in the lithiated-spinel structure.

The scattering intensity variation observed in the $\{111\}$ planes of the lithiated-spinel structure can be related to the cation distribution through the structure factors of these planes. The magnitude of the structure factor depends on the relative amounts of lithium and cobalt on the octahedral 16c and 16d sites of the lithiated-spinel structure. Based on the single-crystal electron diffraction and X-ray diffraction results, this deviation from the ideal intensity distribution exists without the development of new selection rules beyond those observed for the layered ($R\bar{3}m$) and the lithiated-spinel ($Fd3m$). Such an observation is consistent with the hypothesis that, at least in some crystallites, the structure of LT-$LiCoO_2$ could have a cation distribution which is intermediate between the ideal layered and the ideal lithiated-spinel structures (3, 4).

It has been reported that the lithiated-spinel structure can be converted to the layered structure if the four cobalt atoms on the 16d sites with coordinates $(\frac{1}{4}, \frac{1}{2}, \frac{1}{4})$, $(\frac{1}{4}, 0, \frac{3}{4})$, $(\frac{3}{4}, \frac{1}{2}, \frac{3}{4})$, and $(\frac{3}{4}, 0, \frac{1}{4})$, are transposed with the four lithium atoms on the 16c sites with coordinates $(\frac{1}{4}, 0, \frac{1}{4})$, $(\frac{1}{4}, \frac{1}{2}, \frac{3}{4})$, $(\frac{3}{4}, 0, \frac{3}{4})$, and $(\frac{3}{4}, \frac{1}{2}, \frac{1}{4})$ (15). An intermediate structure is produced when a fraction of these cobalt and lithium ions are transposed. This concept may be tested quantitatively by examining and comparing the intensities of four sets of the $\{111\}$ planes in the lithiated-spinel structure and the (003) planes in the layered structure.

The structure factor $F_{\{111\}}$ and the total scattering intensity $I_{\{111\}}$ for the $\{111\}$ atomic planes of an ideal lithiated-spinel $Li_{16}[Co_{16}]O_{32}$ structure with space group symmetry $Fd3m$ and with the oxygen ions located at $(\frac{1}{4}, \frac{1}{4}, \frac{1}{4})$ have the following relationships with respect to one unit cell:

$$F_{\{111\}} = 8(f_{\text{Co}} - f_{\text{Li}}), \qquad [3]$$

$$I_{\{111\}} \propto 8(F_{\{111\}})^2 = 512(f_{\text{Co}} - f_{\text{Li}})^2, \qquad [4]$$

where f_{Co} is the scattering factor of a cobalt atom and f_{Li} is the scattering factor of a lithium atom. By contrast, the structure factor $F_{(003)}$ and the total scattering intensity $I_{(003)}$ for the (003) atomic planes of a layered structure with space group symmetry $R\bar{3}m$ and with an ideal cubic-close-packed oxygen array (i.e., with the oxygen ions located at $(0, 0, \frac{1}{4})$) have the following relationships with respect to one unit cell:

$$F_{(003)} = 3(f_{\text{Co}} - f_{\text{Li}}), \qquad [5]$$

$$I_{(003)} \propto 2(F_{(003)})^2 = 18(f_{\text{Co}} - f_{\text{Li}})^2. \qquad [6]$$

When considering an equivalent number of atoms in the layered structure to the number of atoms in one unit cell of the lithiated-spinel structure, then

$$F'_{(003)} = 16(f_{\text{Co}} - f_{\text{Li}}), \qquad [7]$$

$$I'_{(003)} \propto 2(F'_{(003)})^2 = 512(f_{\text{Co}} - f_{\text{Li}})^2. \qquad [8]$$

These equations indicate that the total scattering intensity from the (003) reflections in the layered structure equals that from the $\{111\}$ reflections of the lithiated-spinel structure. It should be noted that in this calculation, the oxygen ions of the ideally cubic-close-packed structures do not contribute at all to the intensities of the (003) or the $\{111\}$ reflections.

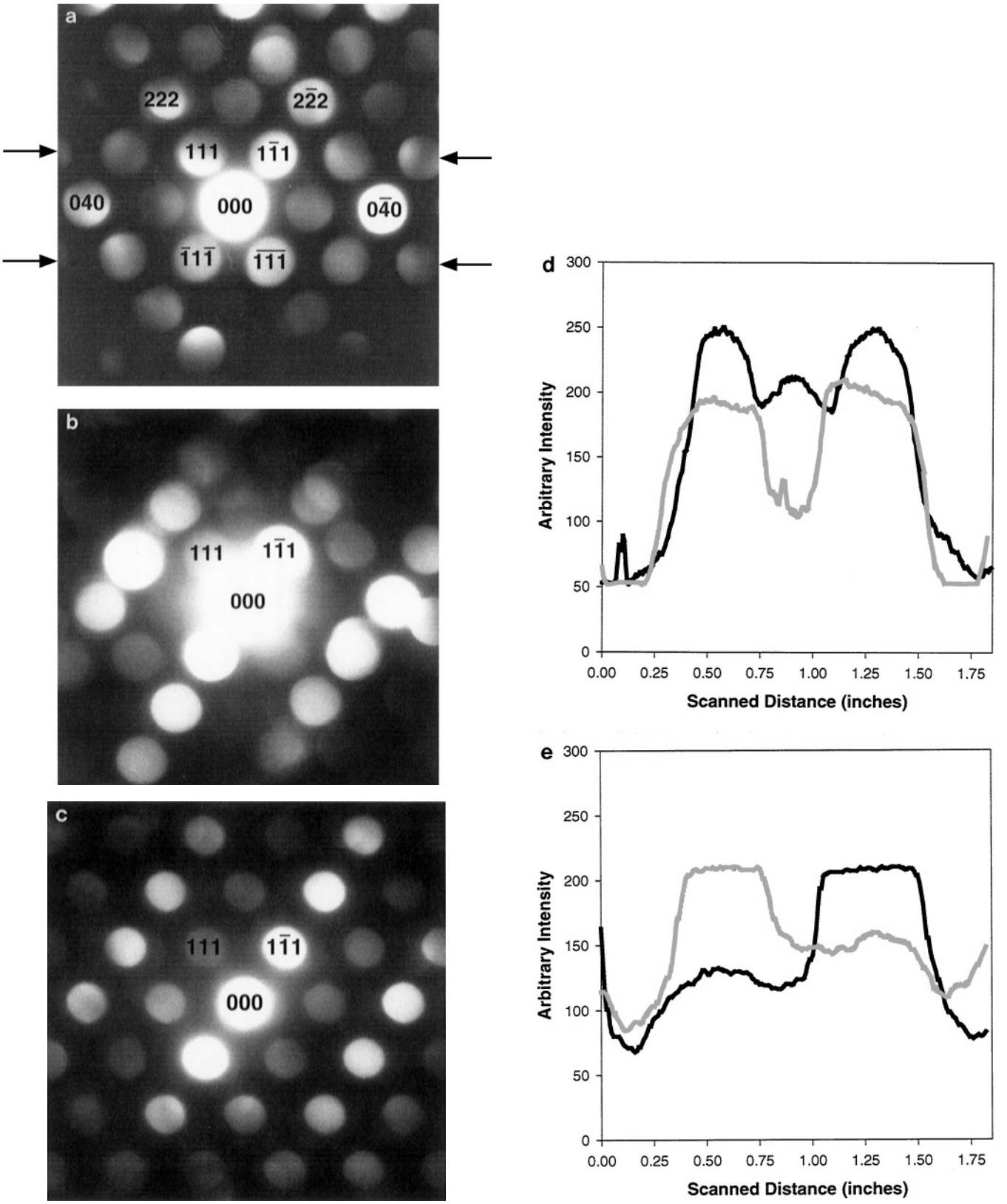

FIG. 7. Single-crystal electron diffraction patterns collected from two LT-$LiCoO_2$ (SS) (a and b) and one LT-$LiCoO_2$ (SG) (c) crystallites, respectively; the scattering intensity profiles (d and e) of the (111) and (1$\bar{1}$1) planes corresponding to (a) and (b), respectively. The scattering intensities are digitized horizontally across the centers of the {111} reflection spots both above and below the center of diffraction (marked by arrows in (a)).

If the positions of 16 lithium and 16 cobalt cations in one unit cell deviate from the ideal lithiated-spinel configuration, then the deviation toward an ideal layered structure can be described by a parameter, x, in the following formula (using spinel notation):

$$\{(Li_{16-4x})_{16c}[Li_{4x}]_{16d}\}_{layer1}\{(Co_{16-4x})_{16d}[Co_{4x}]_{16c}\}_{layer2}O_{32}.$$

When $x = 0$, the structure has the ideal lithiated-spinel configuration, $(Li_{16})_{16c}[Co_{16}]_{16d}O_{32}$, or $(Li_2)_{16c}[Co_2]_{16d}O_4$. When $x = 1$, the structure has the ideal layered configuration, $\{(Li_{12})_{16c}[Li_4]_{16d}\}_{layer1}\{(Co_{12})_{16d}[Co_4]_{16c}\}_{layer2}O_{32}$ (alternatively, in the layered notation, $(Li_3)_{3a}[Co_3]_{3b}O_6$). The magnitude of the structure factor and the scattering intensity for the set of the $\{111\}$ planes with an increasing cobalt density, e.g., the $(1\bar{1}1)$ reflection in Fig. 7b, c, can be described as a function of x:

$$F_{(1\bar{1}1)} = (8f_{Co} + 8xf_{Co} - 8f_{Li} - 8xf_{Li}), \quad [9]$$

$$I_{(1\bar{1}1)} \propto 128(1 + x)^2(f_{Co} - f_{Li})^2. \quad [10]$$

The magnitudes of the structure factors and the scattering intensities for each of the other three sets of the $\{111\}$ planes with decreasing cobalt densities, e.g., the (111) reflection in Fig. 7b, c, can also be described as a function of x:

$$F_{(1\bar{1}1)} = (8f_{Co} - 8xf_{Co} - 8f_{Li} + 8xf_{Li}), \quad [11]$$

$$I_{(111)} \propto 128(1 - x)^2(f_{Co} - f_{Li})^2. \quad [12]$$

The ratio between the scattering intensities of the (111) and $(1\bar{1}1)$ planes, denoted as m, can be related to x by the following equation:

$$m = I_{(111)}/I_{(1\bar{1}1)} = \frac{(1 - x)^2}{(1 + x)^2}. \quad [13]$$

The ratio m is plotted as a function of x, as shown in Fig. 8. It should be noted that m decreases as x increases, i.e., when the specific occupancies of lithium and cobalt ions in the structure vary from the lithiated-spinel to the layered configuration.

Using the m–x relationship in Fig. 8, it is possible to determine the values of x, i.e., the degree of structural variation between the layered and the lithiated-spinel configurations, by measuring the relative intensity ratios of the $\{111\}$ reflections. The caveat to this approach is that the dynamical diffraction conditions often encountered in transmission electron microscopy studies would tend to reduce the intensity differences among the $\{111\}$ reflections. However, the crystallites in this study are small (thin) and there is a deviation from the exact Bragg condition in the zone axis patterns. Taken together with the experimental fact that the variations in the $\{111\}$ scattering intensity are observed, it is apparent that the diffraction conditions in this study are consistent with those described in the kinematical approximation.

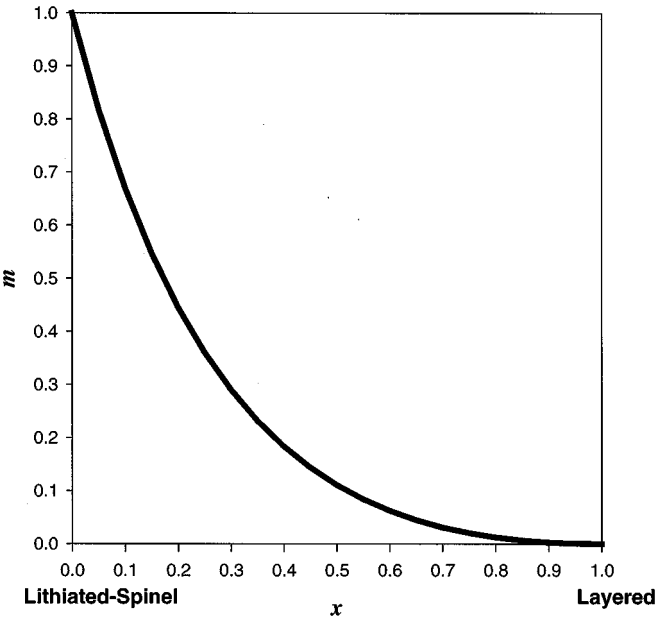

FIG. 8. A plot of variable m as a function of x.

The scattering intensity profiles of the (111) and $(1\bar{1}1)$ reflections in Fig. 7a–c were digitized along the [010] direction. The intensity profiles of the $\{111\}$ reflections in Fig. 7a, b are shown in Fig. 7d and e, respectively. The scattering intensity ratios of (111) and $(1\bar{1}1)$ reflections of LT-$LiCoO_2$ crystallites can be calculated from these digitized profiles. The scattering intensity ratios of the (111) and $(1\bar{1}1)$ planes in Fig. 7a–c, i.e., the values of m, are found to be 0.96, 0.25, and 0.29, respectively; the corresponding values of x, as determined from Fig. 8, are 0.02, 0.33, and 0.30, respectively. It is noted that the electron diffraction pattern in Fig. 7a corresponds to a structure with site occupancies of cations that are almost identical to those of the ideal lithiated-spinel. By contrast, the electron diffraction patterns in Fig. 7b, c corresponds to a structure with a cation distribution between the ideal lithiated-spinel and layered configurations.

The number of single-crystal electron diffraction patterns collected from LT-$LiCoO_2$ (SS) and LT-$LiCoO_2$ (SG) is plotted as a function of x in Fig. 9a and b, respectively. It should be pointed out that there are significantly more crystallites that have a configuration closer to the lithiated-spinel structure ($x < 0.5$) than to the layered structure ($x > 0.5$) in both samples. This result confirms that the lithiated-spinel structure is the major phase in LT-$LiCoO_2$ products. It has

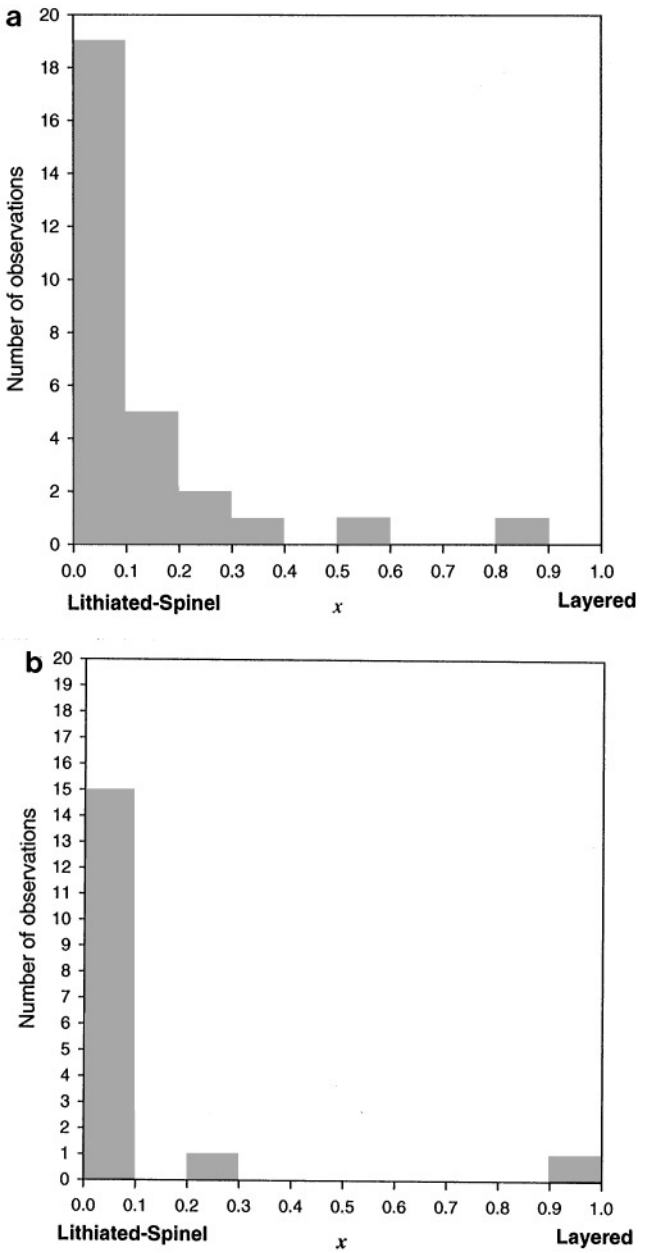

FIG. 9. Number of single-crystal electron diffraction patterns as a function of x for (a) LT-$LiCoO_2$ (SS) and (b) LT-$LiCoO_2$ (SG).

been reported in previous studies (1, 3, 4) that LT-$LiCoO_2$ positive electrodes have very poor electrochemical properties in lithium rechargeable cells. The poor electrochemical behavior of LT-$LiCoO_2$ electrodes can be attributed to the intermediate cation distribution between the layered and the lithiated-spinel structures shown in Fig. 9. This is because the mixing of cobalt and lithium ions in the layered or lithiated-spinel $LiCoO_2$ structures will restrict the two-dimensional or three-dimensional pathways for lithium diffusion that are normally accessible in the ideal layered and ideal spinel structures, respectively. This intermediate cation distribution between the lithiated-spinel and layered structures present in LT-$LiCoO_2$ products also suggests the thermodynamic instability of the lithiated-spinel structure. Significantly, a separate study has shown that prolonged heating (>3 months) of LT-$LiCoO_2$ (SS) samples at 400°C converts a significant amount of the lithiated-spinel phase to the ideal layered configuration (16). This phenomenon emphasizes the thermodynamic stability of the high-temperature HT-$LiCoO_2$ phase with the layered structure ($R\bar{3}m$).

The $\langle 001 \rangle$ single-crystal diffraction patterns collected from LT-$LiCoO_2$ (SS) and LT-$LiCoO_2$ (SG) samples are compared in Fig. 10. The electron diffraction pattern of

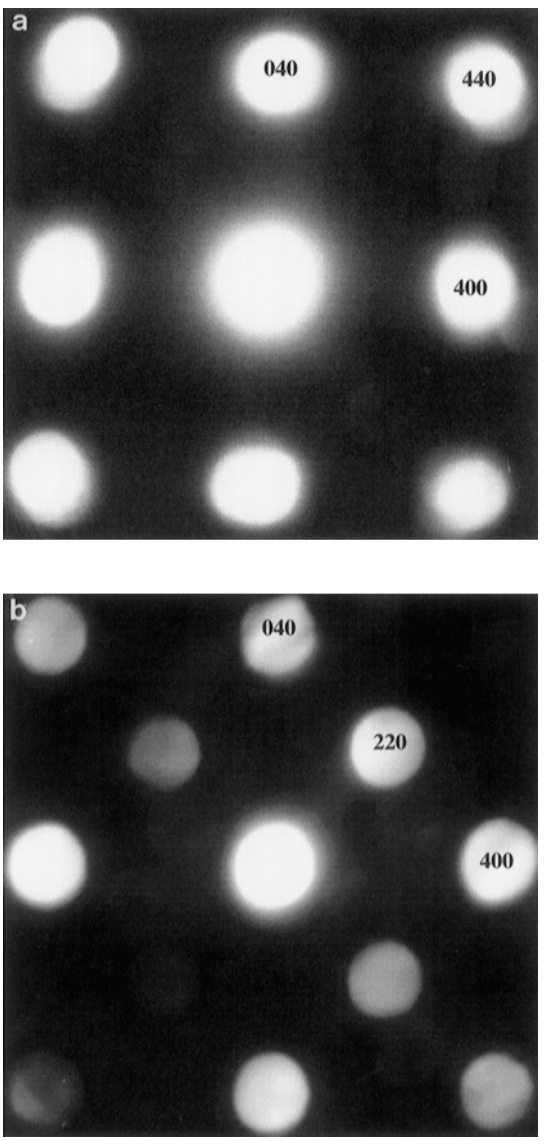

FIG. 10. Single-crystal electron diffraction patterns of (a) the lithiated-spinel structure along the $\langle 001 \rangle$ direction in the LT-$LiCoO_2$ (SS) and (b) $Li_zCo_{3-z}O_4$ ($z \approx 0$) along the $\langle 001 \rangle$ direction in the LT-$LiCoO_2$ (SG).

LT-$LiCoO_2$ (SS) (Fig. 10a) is indexed in a manner consistent with the selection rules of the lithiated-spinel structure. As expected, the forbidden $\{220\}$ reflections were not evident for the lithiated-spinel $Li_2[Co_2]O_4$ structure. Surprisingly, these reflections were evident in 33% of the $\langle 001 \rangle$ diffraction patterns collected from the LT-$LiCoO_2$ (SG) crystallites (Fig. 10b). The presence of these reflections was attributed to the presence of a second spinel phase with composition $Li_zCo_{3-z}O_4$ ($z \approx 0$) within the sample, having lithium and/or cobalt on tetrahedral (8a) sites. The weak $\{220\}$ peak ($I_{220}/I_{111} = 0.04$) marked by an arrow was also visible in the X-ray powder diffraction pattern (indexed to the lithiated-spinel structure) of LT-$LiCoO_2$ (SG) product heated for no more than 2 days at 400°C (Fig. 11a); the (220) peak ($I_{220}/I_{111} = 0.01$) nearly disappeared on annealing the product at the same temperature for a further two days (Fig. 11b). These experiments and data highlight the complexity of the reaction process during synthesis at 400°C and the formation of metastable reaction products with a variety of possible compositions.

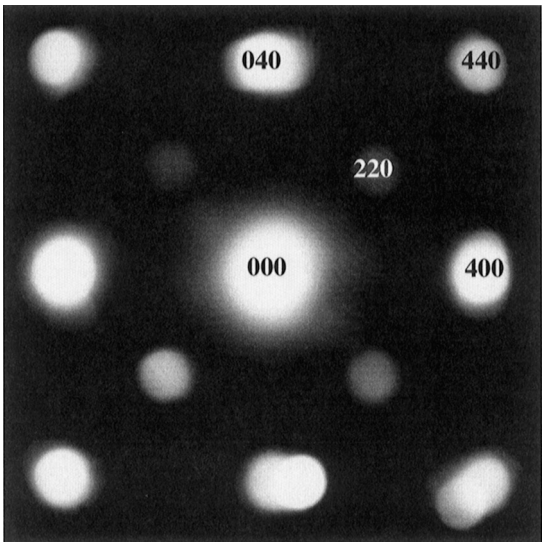

FIG. 12. A single-crystal electron diffraction pattern collected from the acid-delithiated $Li_{0.38}CoO_2$ sample indexed along the $\langle 001 \rangle$ direction according to the spinel structure (*Fd3m*).

Convergent Beam Electron Diffraction Analysis of Acid-Delithiated LT-$Li_{0.38}CoO_2$ (SS)

Electron diffraction analysis of LT-$Li_{0.38}CoO_2$ (SS) was undertaken on separate crystallites within one sample. The $\langle 100 \rangle$ single-crystal diffraction patterns collected from different crystallites were identical; they could be indexed in accordance with spinel symmetry (*Fd3m*), as shown in Fig. 12. The presence of the weak $\{220\}$ reflections is expected for a spinel-type structure $Li_{0.8}[Co_2]O_4$ in which the tetrahedral sites are occupied by lithium. This finding confirms the results of an earlier structure analysis of $Li_{0.8}[Co_2]O_4$ with neutron diffraction data (4). Electron diffraction analysis of $Li_{0.8}[Co_2]O_4$ also found that the variation in the scattering intensity described in Fig. 7b, c were not present. This indicates that the intermediate cation distribution between spinel and the layered structure was removed during acid-delithiation and only the spinel configuration remained. Therefore, it is believed that improved electrochemcial behavior of $Li_{0.8}[Co_2]O_4$ electrodes is attributed to the opening of three-dimensional pathways in the acid-delithiated $Li_{0.8}[Co_2]O_4$ by removing the cobalt ions in the pathways during acid-delithiation (1–5).

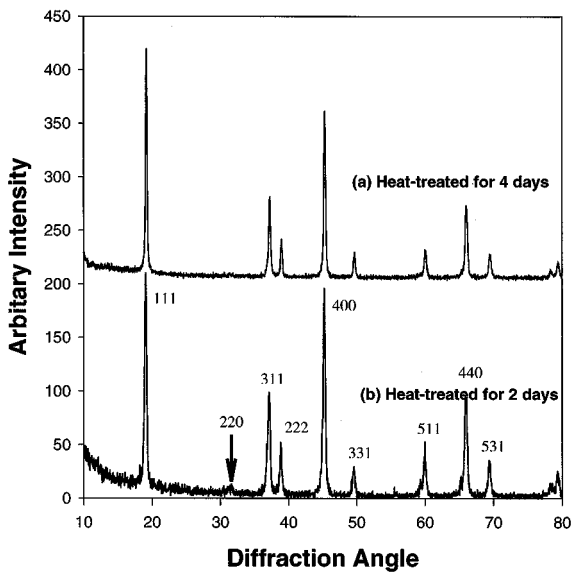

FIG. 11. X-ray diffraction patterns of LT-$LiCoO_2$ products prepared by the sol–gel process: (a) heat-treated at 400°C for 2 days and (b) heat-treated at 400°C for 4 days.

CONCLUSIONS

X-ray diffraction and single-crystal electron diffraction analyses have shown that both the layered and the lithiated-spinel configurations exist in LT-$LiCoO_2$ samples prepared by either the solid-state reaction or the sol–gel process. A cation distribution, $\{(Li_{16-4x})_{16c}[Li_{4x}]_{16d}\}_{layer1}\{(Co_{16-4x})_{16d}[Co_{4x}]_{16c}\}_{layer2}O_{32}$, which is intermediate between an ideal layered and an ideal lithiated-spinel configuration has been detected in both LT-$LiCoO_2$ samples. A single-crystal electron diffraction analysis has demonstrated that acid-delithiation of LT-$LiCoO_2$ results in a nanoporous product; it has confirmed that the reaction results in a defect spinel with composition $Li_{0.8}[Co_2]O_4$. The intermediate cation distribution between spinel and the layered structures was removed during acid-delithiation and only the spinel configuration remained in the $Li_{0.8}[Co_2]O_4$ product. The

structural features of the LT-$LiCoO_2$ and $Li_{0.8}[Co_2]O_4$ products account for their electrochemical properties when they are used as positive electrodes in lithium rechargeable cells.

ACKNOWLEDGMENT

Support from the U.S. Department of Energy's Advanced Battery Program, Chemical Sciences Division, Office of Basic Energy Sciences, under Contract W-31-109-Eng-38 is gratefully acknowledged.

REFERENCES

1. R. J. Gummow, M. M. Thackeray, W. I. F. David, and S. Hull, *Mater. Res. Bull.* **27,** 327 (1992).
2. R. J. Gummow and M. M. Thackeray, *Solid State Ionics* **53,** 681 (1992).
3. R. J. Gummow, D. C. Liles, and M. M. Thackeray, *Mater. Res. Bull.* **28,** 235 (1993).
4. R. J. Gummow, D. C. Liles, M. M. Thackeray, and W. I. F. David, *Mater. Res. Bull.* **28,** 1177 (1993).
5. R. J. Gummow and M. M. Thackeray, *J. Electrochem. Soc.* **140,** 3365 (1993).
6. W. Li, J. N. Reimers, and J. R. Dahn, *Phys. Rev. B* **49,** 826 (1994).
7. E. Rossen, J. N. Reimers, and J. R. Dahn, *Solid State Ionics* **62,** 53 (1993).
8. W. Huang and R. Frech, *Solid State Ionics* **86,** 395 (1996).
9. B. Garcia, P. Barboux, F. Ribot, A. Kahn-Harari, L. Mazerolles, and N. Baffier, *Solid State Ionics* **80,** 111 (1995).
10. H. J. Orman and P. J. Wiseman, *Acta Crystallogr. C* **40,** 12 (1984).
11. W. D. Johnston, R. R. Heikes, and D. Sestrich, *J. Phys. Chem. Solids* **7,** 1 (1958).
12. K. Mizushima, P. C. Jones, P. J. Wiseman, and J. B. Goodenough, *Mater. Res. Bull.* **15,** 783 (1983).
13. B. D. Cullity, "Elements of X-ray Diffraction," 2nd ed., p. 102. Addison-Wesley, Reading, MA, 1978.
14. Y. Shao-Horn, Y. Ein-Eli, A. D. Robertson, W. F. Averill, S. A. Hackney, and W. F. Howard, *J. Electrochem. Soc.* **145,** 16 (1998).
15. R. J. Gummow, Ph.D. Dissertation, University of Cape Town, South Africa, 1993.
16. Y. Shao-Horn, S. A. Hackney, C. S. Johnson, A. J. Kahaian, and M. M. Thackeray, Presented at the Fall Meeting, Materials Research Society, Boston (December 1997).